Soft Matter

RSC Publishing

PAPER

View Article Online
View Journal | View Issue

Pore-size entropy of random hard-sphere packings

Cite this: *Soft Matter*, 2013, **9**, 3361

Vasili Baranau, Dzmitry Hlushkou, Siarhei Khirevich and Ulrich Tallarek*

We introduce a method for calculating the entropy of random hard-sphere packings, also referred to as pore-size entropy. The method is applicable to packings of monodisperse or polydisperse spheres as well as non-spherical particles. Pore-size entropy allows us to analyze the packing microstructure and provides deep insight into the traditional concept of pore-size distribution. Specifically, the logarithm of the pore-size distribution's tail area is equal to the packing entropy. We reveal a local minimum in the plot of pore-size entropy *vs.* packing density (φ) for monodisperse frictionless sphere packings at a critical density of $\varphi_C \approx 0.65$, independent of the employed packing generation protocol (Lubachevsky–Stillinger, Jodrey–Tory, and force-biased algorithms), which is a density with minimal number of available packing configurations. This entropy minimum is followed by an entropy increase as φ increases up to ~0.68, corresponding to the emergence of crystalline structures in the coexistence region; beyond this packing density the entropy decreases again. In a complementary study we modify the Lubachevsky–Stillinger protocol and reproduce the random-close packing limit at $\varphi_{RCP} \approx 0.64$. We conclude that $\varphi_{RCP} \approx 0.64$ is the jamming point of the glassy states with the lowest density, whereas $\varphi_C \approx 0.65$ is the jamming point of the densest glassy state (the ideal glass state).

Received 15th October 2012
Accepted 28th January 2013

DOI: 10.1039/c3sm27374a

www.rsc.org/softmatter

I Introduction

Numerous authors have demonstrated structural changes in random packings of monosized frictionless hard spheres (*e.g.*, the onset of crystallization) for solid volume fractions φ ranging from 0.646 to 0.65, which is sometimes believed to indicate the random-close packing (RCP) limit or even used as a definition of the latter.[1–6] The fact that packings of monosized spheres are random up to a density of $\varphi \approx 0.65$ and start arranging into crystalline structures for higher densities suggests that an entropic measure could be helpful in defining, detecting, and understanding the properties of this transition. Numerous papers have introduced and utilized entropy for hard-sphere systems.[1,7–19] On the other hand, one of the tools for description and investigation of packing properties is the pore-size distribution, also called the nearest-surface distance distribution or void-size distribution; introduced, examined, and applied to hard-sphere packings in many publications.[20–28]

The main objective of this paper is to link the packing entropy to the nearest-surface distance distribution, providing a better understanding of the latter. The entropic measure that we derive is numerically robust and can easily be applied to monodisperse and polydisperse sphere packings, as well as to non-spherical[29,30] particles; furthermore, it does not depend on *a priori* parameters (*e.g.*, Debye length,[1,17] Planck length,[8–10,12] or others), presenting a convenient and powerful tool for a detailed analysis of packing properties, including preparation protocol-specific disorder and structural transitions upon compaction.

In the assumption of equiprobable microstates at a given packing density[7,17,31] the entropy of a packing is the logarithm of the total number of valid packing configurations described by particle coordinates and radii, which is proportional to the probability of finding a valid packing (*i.e.*, without particle intersections) among all packing configurations. We assume that the probability of successful insertion of a particle into a valid packing is equal to the probability of finding a valid packing among all packing configurations. We subsequently estimate the probability of a successful particle insertion by building a pore-size distribution for a packing, fitting it with a Gaussian curve[25] and calculating the area under the tail of this distribution, starting from the mean particle radius. Therefore, the pore-size entropy also provides deep insight into the traditional concept of the pore-size distribution; specifically, the logarithm of its tail area equals the entropy of a packing.

To test the validity of this approach we apply the entropy measure in a wide range of packing density ($\varphi = 0.6$–0.7) to computer-generated monodisperse frictionless sphere packings, each containing 10 000 spheres residing in a cubic box with periodic boundary conditions in all directions. Packings were generated with (i) the Lubachevsky–Stillinger (LS) algorithm,[32] (ii) the Jodrey–Tory (JT) algorithm,[33,34] and (iii) a force-biased algorithm (FBA).[35,36]

The pore-size entropy reveals a pronounced minimum at a critical density of $\varphi_C = 0.647$–0.651, in agreement with structural transition densities reported previously (we will also refer to this minimum as a "structural transition density"). There still

Department of Chemistry, Philipps-Universität Marburg, Hans-Meerwein-Strasse, 35032 Marburg, Germany. E-mail: tallarek@staff.uni-marburg.de; Fax: +49 6421 28 27061; Tel: +49 6421 28 25727

remains an open question on how this structural transition density is related to the generally accepted RCP limit ($\varphi_{RCP} \approx 0.64$) obtained experimentally and by the direct generation of jammed configurations.[8,11,37–42] In this paper, by the RCP limit we will understand the infinite-pressure limit of the least dense glassy states,[43] which can be obtained by the generation of mechanically stable packings in the infinitely large compression-rate limit (which indeed produces packings at $\varphi_{RCP} \approx 0.64$).[43–45] By jamming we understand collective jamming in packings of frictionless particles[46–49] (equivalent to mechanical stability,[8] isostaticity,[10,39–41,46,50–60] and infinite pressure in systems of particles supplied with velocity[61]).

We will discuss the relationship between the structural transition density (φ_C) and the RCP limit (φ_{RCP}) in Section IV, parts C and D. To resolve the issue of the two density estimates (φ_C and φ_{RCP}) we amend the Lubachevsky–Stillinger generation protocol to completely equilibrate sphere packings (*i.e.*, conduct molecular dynamics simulations with zero compression rate until the pressure is stationary) after every 2×10^4 collisions with compression. This amendment allows systematic reproduction of the RCP limit at $\varphi_{RCP} \approx 0.64$ with fast compressions. We are not aware of any work that recovers both characteristic packing densities ($\sim$0.64 and $\sim$0.65) with the same packing generation protocol.

The last result suggests that the structural transition observed at $\varphi_C = 0.647$–0.651 and the RCP limit at $\varphi_{RCP} \approx 0.64$ are distinct phenomena, which cannot be justified by a difference in the preparation protocols. We explain this observation on the basis of a picture proposed in a review by Parisi and Zamponi.[43] While $\varphi_{RCP} \approx 0.64$ corresponds to the jammed configurations of the least dense glassy states (φ_{th} in this review), $\varphi_C = 0.647$–0.651 corresponds to the jammed configuration of the densest glassy state (φ_{GCP} in this review).

We provide an overview of the employed packing generation methods in Section II; the pore-size entropy measure is derived and its connection to the pore-size distribution is explained in Section III; results, discussion, and conclusions are provided in Sections IV and V.

II Packing generation methods

In this paper, we analyze computer-generated packings, each containing 10 000 spheres residing in a cubic box with periodic boundary conditions in all directions. Packings of monodisperse frictionless spheres were generated with (i) the Lubachevsky–Stillinger (LS) algorithm[32] using codes from Skoge *et al.*[62] and Donev *et al.*,[29] (ii) the Jodrey–Tory (JT) algorithm,[33,34] and (iii) a force-biased algorithm (FBA),[35,36] which is a modification of the JT algorithm also used by several other authors.[1,5,11,63]

The LS algorithm is, in principle, a molecular dynamics simulation aiming at absolutely elastic hard sphere movement modeling, which starts from a random distribution of spheres in a given simulation box of radius sufficiently small to avoid sphere intersections. In the course of event-driven molecular dynamics simulation the particle radii are gradually increased with a certain expansion rate until the pressure, produced by particle momentum, reaches a predefined large enough value. The lower the expansion rate, the denser will be the final configuration. For monodisperse particles, the LS algorithm can easily produce almost perfectly crystalline packings. The maximal reduced pressure in a packing was 10^{12} and the spheres' growth rate varied from 10^{-5} to 0.2. The total number of packings generated with the LS algorithm was 230.

The JT algorithm also starts from a random distribution of sphere (particle) centers in a simulation box. Each sphere is supplied with an inner diameter chosen to be proportional to the desired sphere diameter and to make the particles in the closest pair touch each other with their inner diameter shells, and consequently to avoid any particle intersections in a packing. Alternatively, a single inner diameter ratio can be specified for the entire packing as the ratio of inner diameters to the desired particle diameters. Similarly, a packing is supplied with an outer diameter ratio, initially larger than unity (so that each sphere has an outer diameter proportional to and larger than the desired one). A common approach for the outer diameter ratio initialization is to ensure that the total volume of the particles is equal to the box volume. At each iteration, the following steps are performed: (i) the pair of particles with the largest outer diameter intersection is found; (ii) particles of this pair are spread along their intersection line so that the intersection of outer shells is completely removed (but new intersections with other particles may occur); (iii) the outer diameter ratio is decreased according to some contraction rate; and (iv) the inner diameter ratio is updated to make particles in the closest pair touch each other with their inner diameter shells.

In its classical version the JT algorithm terminates when the outer diameter ratio is equal to the inner diameter ratio; the lower the outer diameter ratio contraction rate, the denser becomes the final configuration. In the current paper we use a modified termination condition for JT packings and stop the generation when the inner diameter ratio is equal to unity, which allows us to achieve the exact required density. We chose the contraction rate (k in the original paper[33]) to be 10^{-5}. The algorithm can easily produce monodisperse packings up to the structural transition density φ_C. To overcome this limit we restarted the generation several (up to 20) times using the particle positions from the previous run as the starting configuration.

The FBA is a modification of the JT algorithm, which can be classified as a "collective rearrangement" method. The initial distribution of particles is also random and particles are supplied with inner and outer diameters of the same meaning. Particles are also supplied with elastic potential (usually of the third order by the overlap distance),[36] which is cut-off at the outer particle shell. Therefore, it is possible to compute particle forces (of the second order by the overlap distance) between each particle pair with intersecting outer shells, as well as net forces for each particle. The iteration proceeds as follows: (i) all the particle forces and net forces for each particle are determined; (ii) all particles are displaced by distances proportional to their net forces and in the direction of net forces; (iii) the outer diameter ratio is decreased according to some contraction rate; and (iv) the inner diameter ratio is updated so that inner

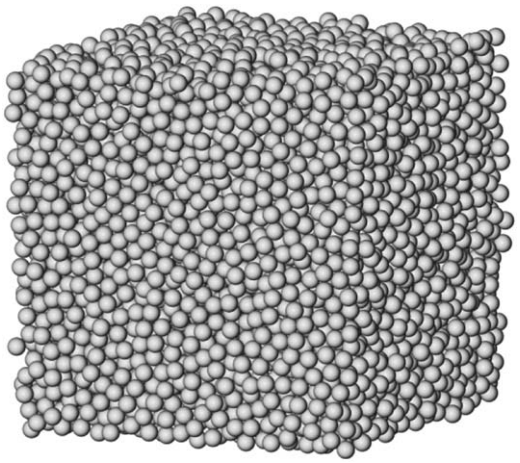

Fig. 1 A random packing of 10 000 monosized spheres at a solid volume fraction of $\varphi = 0.64$, generated with the force-biased algorithm.

diameter shells of the particles in the closest pair touch each other. In this paper, we modify a standard termination condition for the algorithm and stop the generation when one of the two criteria is satisfied: (i) the outer diameter ratio is equal to the inner diameter ratio; or (ii) the inner diameter ratio is equal to unity (if the first condition has not yet been met). The lower the outer diameter ratio contraction rate, the denser the final configuration; in contrast to the JT algorithm this algorithm can easily overcome the structural transition density φ_C of monodisperse sphere packings.

The parameters of the FBA were the following (notation taken from Bezrukov *et al.*[36]): force scaling factor, $\rho = 0.5$; values of τ control the final density and span from 4×10^3 to 7×10^6. The total number of packings generated with the FBA was 230. An exemplary sphere packing at a packing density of $\varphi = 0.64$ is presented in Fig. 1.

Here, we point out a connection between the FBA and energy minimization protocols used in many papers.[39–41,50,52] In these protocols, the particles are supplied with elastic potential and are initially placed randomly in a simulation box. The following steps are performed on each iteration of the algorithm: (i) particles are displaced to find local minima of the elastic energy associated with intersections employing a standard optimization method, and (ii) the box is expanded to decrease particle overlaps.

A decrease of the outer diameter ratio in the FBA is equivalent to a box expansion in energy minimization protocols. Furthermore, the displacement of particles in the direction of net forces in the FBA can be interpreted as the simplest version of potential energy minimization through the steepest descent method. Therefore, the FBA corresponds to simultaneous box expansion and intersection energy minimization and, in principle, is very similar to energy minimization protocols.

III Pore-size entropy

In this section a new method for calculation of the granular matter entropy (called pore-size entropy) is introduced. It can be easily applied to monodisperse and polydisperse hard-sphere packings as well as to packings of non-spherical[29,30] particles. Furthermore, it does not depend on *a priori* parameters (*e.g.*, Debye length,[1,17] Planck length,[8–10,12] or others) and allows us to directly analyze packing properties like structural transition and packing protocol-specific disorder.

We now provide an overview of the derivation of the entropic measure. In the assumption of equiprobable microstates at a given packing density[7,17,31] the entropy of a packing is the logarithm of the total number of valid packing configurations described by particle coordinates and radii, which is proportional to the probability of finding a valid packing (*i.e.*, without particle intersections) among all packing configurations. We assume that the probability of successful insertion of a particle into a valid packing is equal to the probability of finding a valid packing among all packing configurations. We subsequently estimate the probability of a successful particle insertion by building a pore-size distribution for a packing, fitting it with a Gaussian curve[25] and calculating the area under the tail of this distribution, starting from the mean particle radius. Thus, this measure also provides deep insight into the traditional concept of pore-size distribution; specifically, the logarithm of its tail area equals the entropy of a packing. We start the derivation from monosized packings and extend the idea to polydisperse packings.

A Phase space description

Each packing configuration of N monosized particles can be represented as a point in a $3N$-dimensional packing phase space (3 coordinates per particle center). For packing box sides L_x, L_y, and L_z, respectively, the total phase space volume equals $V_{tot} = (L_x L_y L_z)^N$. If a given point in the phase space corresponds to at least one physical overlap between particles, it is unavailable. The true Gibbs entropy of an N-particle packing ensemble with a given density is determined by the volume of the phase space available to the packings. The structure of basins of attraction for available states in small packings of hard particles has been studied in several recent papers.[64,65]

To construct the entropy, we uniformly discretize the entire phase space by M points, for example, through discretization of each of the packing box dimensions by M_x, M_y, and M_z points, respectively, in which case $M = (M_x M_y M_z)^N$. With the assumption of equiprobable system microstates,[7,17,31] the entropy S of the packing ensemble is calculated as

$$S = \ln(M_{avail}) = \ln(M p_{avail}) = \ln(M) + \ln(p_{avail}), \quad (1)$$

where M_{avail} is the total number of valid phase space points and p_{avail} is the probability of encountering an available state in the phase space (the density of available states).

To assess relative entropy values we do not need the constant term $\ln(M)$ in the computation, as it does not depend on the packing protocol, packing volume fraction, particle size distribution, *etc.*, which leads to

$$S_{avail} = \ln(p_{avail}), \quad (2)$$

thus allowing infinitely precise discretization. We add a subscript "avail" to the entropy to emphasize that it is a contribution to the entropy and will bear negative values.

This formula can be treated without the notion of entropy as follows: the phase space region for a packing of a given size is characterized by the probability of encountering an available hyperpoint in that region, which we assess through the logarithm in eqn (2).

We point out a distinction between a "strong" form of the equiprobability assumption and a "weak" one. The strong form implies that valid packing configurations in the entire range of density are equally probable (*i.e.*, the phase space has an additional dimension of packing density or particle diameter); the weak form implies that packing configurations are equiprobable for any given density, though configuration (microstate) probabilities for different densities may not be equal. The discussion in the present paper relies on the weak form of the equiprobability assumption, whereas configurations for distinct densities may have drastically different probabilities.

We note that different protocols may yield distinct entropy values even if the equiprobability assumption holds for each of the protocols. This may happen if the protocols sample different subregions of the phase space and can reach different numbers of valid configurations, though valid reachable configurations for each of the protocols are equiprobable.

B Slicing assumption

Each packing of N monosized particles can be viewed as a 3-dimensional slice of a $3(N+1)$-dimensional packing phase space of $N+1$ particles, with 3 coordinates of the last particle left unconstrained.

This slice may be viewed as a $3(N+1)$-dimensional thin layer in a phase space, given that the first N particles are allowed to change their coordinates slightly by the discretization length. The volume of this layer is $V_{\text{layer}} = L_xL_yL_z(L_xL_yL_z/M_xM_yM_z)^N$.

As far as the packings are random and uniform, we predict that the probability p_{avail} of encountering an available hyperstate in this thin hyperlayer is very close to the one computed from the entire phase space (if the number of particles in the packings is sufficiently large). In other words, the density of available states in the hyperlayer is equal to the density in the entire packing. As far as the first N particles have no intersections and their coordinates are fixed, and just the last particle can be moved, each available hyperstate actually corresponds to the successful insertion of the $(N+1)^{\text{th}}$ particle in the packing of N particles.

Thus, one can estimate p_{avail} by taking a computer-generated packing and trying to insert a test particle in the voxels of the discrete mesh of $M_xM_yM_z$ points (equivalent to the successful estimation of the insertion probability, p_{insert}), which yields

$$p_{\text{insert}} = p_{\text{avail}}. \tag{3}$$

This procedure is still numerically challenging and depends on the discretization. The slicing assumption reflects a traditional approach in statistical physics, when properties of the system ensemble are determined from a single large enough system.

If it turns out that the weak form of the equiprobability assumption does not hold in the thermodynamic limit, the entropy computed by a single packing will be distinct from the true entropy computed as $S = -\sum p_i \log(p_i)$, where the sum is taken over all the packing states and p_i is the state probability. Instead, the entropy will reflect the value for the phase space, as if it were constructed from the equiprobable configurations which are very similar in structure to the current packing (so the current packing is a typical one). The discrepancy between actual and estimated entropies will depend on the probability distribution. Even in this case the measure that we will derive may serve as a convenient tool for investigation of the packing microstructure.

We are unable to restrict packing configurations accounted for in the entropy values only to jammed configurations due to the slicing assumption; therefore, the entropy will be comprised of configurational and vibrational contributions, *i.e.*, mechanically stable and unstable, but still valid, configurations will be counted to give the entropy value.

C Insertion probability

The following method for estimating the insertion probability was derived. We randomly generate a sufficient number of points uniformly inside the packing and determine the maximum radius of a sphere to be inserted at a given point by the distance from the nearest particle surface. If a point resides inside an initially generated particle, the insertion radius is still equal to the distance from the surface, but it carries a negative sign.

If the coordinates of such a random point are $\boldsymbol{r}$, the nearest neighbor center coordinates are $\boldsymbol{r}_{\text{neigh}}$, and the nearest neighbor radius is R, the insertion radius is $r_{\text{insert}} = ||\boldsymbol{r} - \boldsymbol{r}_{\text{neigh}}|| - R$. Then we build an insertion radii distribution for the entire packing and estimate the probability density function $f_{\text{pore}}(r)$ of successful insertion of a sphere with a given radius. This distribution is described in many papers as the pore-size distribution.[20–28]

The probability of successful insertion of a sphere with radius r_{insert} is given by the tail area of the pore-size distribution, starting from r_{insert}:

$$p_{\text{insert}}(r_{\text{insert}}) = \int_{r_{\text{insert}}}^{\infty} f_{\text{pore}}(r')\mathrm{d}r'. \tag{4}$$

We follow the work of Schenker *et al.*[25] and approximate the pore-size distribution with a standard Gaussian curve

$$f_{\text{pore}}(r) \approx C\frac{1}{\sigma\sqrt{2\pi}}\exp\frac{(r-\mu)^2}{2\sigma^2}, \quad r>0, \tag{5}$$

$$p_{\text{insert}}(r) \approx C\frac{1}{2}\left(1 - \operatorname{erf}\left(\frac{r-\mu}{\sigma\sqrt{2}}\right)\right), \quad r>0, \tag{6}$$

where μ and σ are parameters determined from the fitting of the pore-size distribution (obtained numerically). Standard distribution fitting techniques are inapplicable, as normal distribution is not exposed for the entire range of radius, just for pores with positive radii. Thus, one can use maximum likelihood fitting for normal distribution truncated above zero.[66] Another possibility is to use a quadratic least-squares fit over the logarithm of the experimentally measured pore-size distribution.

Polynomial coefficients can easily be converted into Gaussian distribution parameters afterwards.

The normalization constant C in eqn (5) and (6) originates from the fact that some pore centers will be generated inside existing particles. As far as the probability of generating a random point in the interparticle void space, *i.e.*, between particles, is equal to the packing porosity (interparticle void volume fraction), $\varepsilon = 1 - \varphi$, the normalization factor satisfies the equation

$$\int_0^\infty f_{\text{pore}}(r)\mathrm{d}r = C\int_0^\infty \frac{1}{\sigma\sqrt{2\pi}}\exp\frac{(r-\mu)^2}{2\sigma^2}\mathrm{d}r = \varepsilon. \quad (7)$$

The insertion probability estimate p_{insert} can be applied to both monodisperse and polydisperse packings.

Fig. 2 shows pore-size distributions for LS-generated random packings of monodisperse particles at different packing densities (φ as indicated), alongside with their Gaussian fits (the particle radius for all packings is 0.5 a.u.). The fit quality is very good, but decreases at increasing φ; coefficients of determination R^2 for the fits in Fig. 2 (computed for distribution tails with pore radii larger than 0.2 a.u.) are 0.9999, 0.9988, 0.9980, and 0.9797 in the order of increasing φ. The reason underlying this trend is that the pore-size distributions are not perfectly Gaussian (eqn (5)); this deviation increases with the packing density. We note in advance that the slight deviations of radii distributions from a perfect bell shape explain the noise in the pore-size entropy plots for packings denser than $\varphi_C = 0.647$–0.651 in Fig. 3.

D Packing entropy

Finally, for monodisperse sphere packings with particle radius r_0 the entropy is computed by combining eqn (2), (3), and (6)

$$S_{\text{avail}} = \ln(p_{\text{avail}}) = \ln\big(p_{\text{insert}}(r_0)\big) = \ln\left(C\frac{1}{2}\left(1 - \text{erf}\left(\frac{r_0-\mu}{\sigma\sqrt{2}}\right)\right)\right). \quad (8)$$

Eqn (8) shows that the entropy of a packing is the logarithm of the pore-size distribution's tail area (starting from the particle radius) and thereby relates the pore-size distribution to packing entropy.

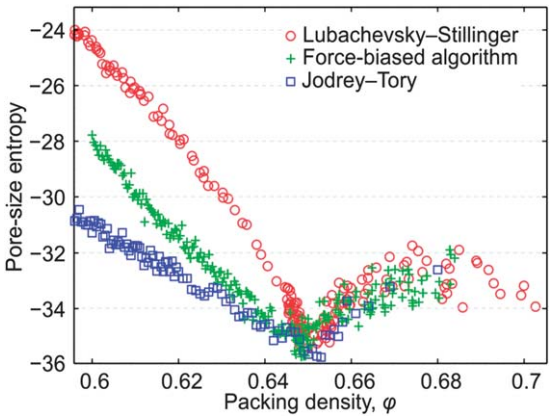

Fig. 3 Pore-size entropy (eqn (12)) *vs.* packing density for monodisperse sphere packings generated with the Lubachevsky–Stillinger algorithm (○), a force-biased algorithm (+), and the Jodrey–Tory algorithm (□).

One can estimate the entropy easily even without fitting of the pore-size distribution as follows. The probability of inserting a particle in a dense packing is extremely low. Therefore, we may substitute the complementary error function from eqn (6) with the first term of its asymptotic expansion:[67]

$$1 - \text{erf}(x) \approx \frac{e^{-x^2}}{x\sqrt{\pi}}. \quad (9)$$

Consequently,

$$S_{\text{avail}} = \ln(p_{\text{insert}}(r_0)) \approx \ln\left(\frac{1}{2\sqrt{\pi}}\right) + \ln(C) - \ln\left(\frac{r_0-\mu}{\sigma\sqrt{2}}\right) - \frac{1}{2}\left(\frac{r_0-\mu}{\sigma}\right)^2. \quad (10)$$

Typical values for the fitting parameters (measured in particle diameters, so that $r_0 = 0.5$) are $\mu = -0.057$ and $\sigma = 0.085$, and a typical value for the normalization constant is

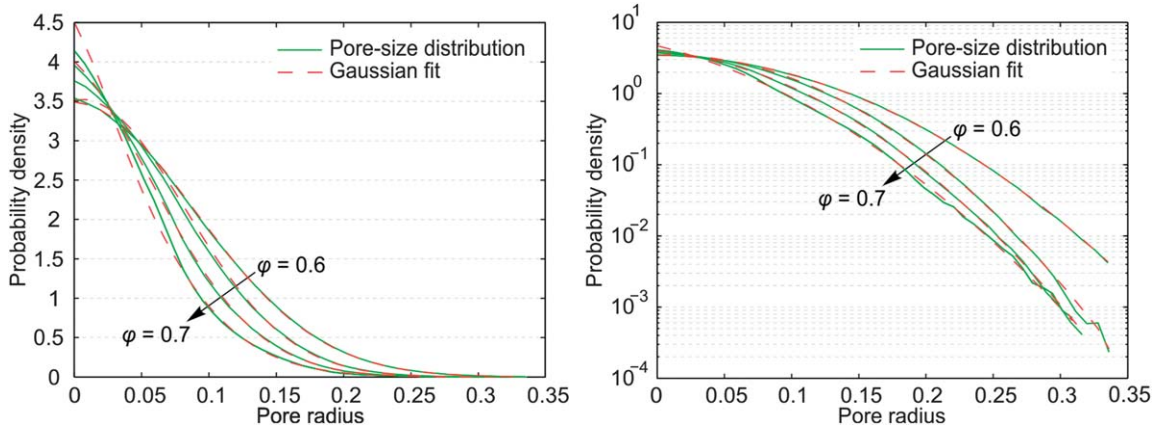

Fig. 2 Probability density functions for pore radii distributions (solid green lines) and their best fits with Gaussian curves (dashed red lines). Left panel: linear scale, right panel: log–linear scale. Packing densities φ along the direction of the arrow: 0.6, 0.6303, 0.6658, 0.7. The packings were generated with the Lubachevsky–Stillinger algorithm. Pore radii were normalized with respect to the particle diameter.

$C = 2$, while a typical entropy value is $S_{\text{avail}} = -25$. Therefore, the last term in eqn (10) is by an order of magnitude larger than the other ones, so we can approximate the entropy as

$$S_{\text{avail}} = \ln\left(p_{\text{insert}}(r_0)\right) \approx -\frac{1}{2}\left(\frac{r_0}{\sigma}\right)^2. \tag{11}$$

Subsequently, we try to compute the insertion probability for particles with smaller radius and to link it to the entropy. Let the smaller radius r be different from the initial particle radius r_0 by the factor α, $r_0 = \alpha r$, then

$$\begin{aligned} S_{\text{avail}} &= \ln\left(p_{\text{insert}}(r_0)\right) \approx -\frac{1}{2}\left(\frac{r_0}{\sigma}\right)^2 = -\frac{1}{2}\left(\frac{\alpha r}{\sigma}\right)^2 \\ &= -\alpha^2\frac{1}{2}\left(\frac{r}{\sigma}\right)^2 \approx \alpha^2 \ln\left(p_{\text{insert}}\left(\frac{r_0}{\alpha}\right)\right). \end{aligned} \tag{12}$$

If there are enough generated pores with a radius larger than r_0/α, we can estimate the insertion probability directly by dividing the number of large-enough pores by the total number of pores and substitute it into eqn (12). This approach benefits from the absence of a distribution fitting, which affects entropy values significantly, as far as $p_{\text{insert}}(r_0)$ is very low. In our simulations we have found that $\alpha = 2$ is sufficient and provides the best trade-off between the required number of large pores and the deviation from eqn (8).

It is straightforward to extend the above formalism to packings of polydisperse particles by using four dimensions per particle in the phase space: three for the particle center coordinates and one for the particle radius. The dimensionality of the phase space of N-particle-packing ensembles is therefore $4N$ and the total phase space volume for the packings is $V_{\text{tot}} = (L_x L_y L_z R_{\max})^N$, where $R_{\max}$ is the largest particle radius supported by the particle size distribution. Eqn (2) still holds, as well as the slicing assumption, although each packing of N polydisperse particles now represents a four-dimensional slice of the phase space, and to estimate the available states density we should try to insert particles of random radii (according to their size distribution) in each point inside the packing. The insertion probability can be approximated with the pore-size distribution as follows

$$p_{\text{insert}} = \int_0^\infty p_{\text{insert}}(r) f_{\text{size}}(r)\mathrm{d}r, \tag{13}$$

where $p_{\text{insert}}(r)$ is determined using eqn (4) and (5), and $f_{\text{size}}(r)$ is the probability density function of the particle radii distribution. The entropy of polydisperse packings is thus equal to

$$S_{\text{avail}} = \ln \int_0^\infty C\frac{1}{2}\left(1 - \operatorname{erf}\left(\frac{r-\mu}{\sigma\sqrt{2}}\right)\right) f_{\text{size}}(r)\mathrm{d}r. \tag{14}$$

It is also feasible to estimate the probability p_{avail} of available packing configurations by trying to insert a particle with number-mean radius into a polydisperse packing, *i.e.*, to calculate the entropy of polydisperse packings using eqn (8) or (12), with r_0 as the number-mean particle radius.

IV Results and discussion

A Pore-size entropy

We now apply the pore-size entropy measure to several types of monodisperse sphere packings (generated as described in Section II) covering a wide range of packing volume fractions φ (Fig. 3). The pore-size entropy is computed using eqn (12) with $\alpha = 2$. The total number of randomly inserted points used for the construction of the pore-size distribution was 10^7 for each packing. We did not remove rattler particles[32] from jammed configurations, though we verified that recursive removal (without updating the packing density[56,59]) of rattler particles with less than four contacts,[59,62,68] which is a minimum number required for mechanical stability, influences the results insignificantly and we therefore do not present separate plots.

Expectedly, the pore-size entropy in Fig. 3 initially decreases with increasing φ, as the amount of available packing configurations decreases due to the higher probability of particle intersections. The entropy reaches a profound local minimum for all packing types at a critical density of $\varphi_C = 0.647$–0.651. This density is associated with the minimal number of available states that can be reached in the course of a physical packing preparation protocol. Indeed, a packing preparation process can be interpreted as moving a point of the complete packing description in a multidimensional phase space. It is tempting to attribute this density φ_C to the RCP limit, but we postpone this discussion until Section IV, part C.

The local minimum at $\varphi_C = 0.647$–0.651 in Fig. 3 is followed by a strong entropy increase upon further compaction of the packings, which is usually explained by the emergence of crystalline regions and releasing portions of the phase space available for new packing configurations.[1] This is due to at least two mechanisms: (i) there is a certain freedom in shifting the particles in crystalline configurations (which is sometimes called vibrational entropy;[43] it is well known that the vibrational entropy for crystals is higher than that for random structures, *e.g.*, liquids); (ii) the existence of crystalline subregions of higher density allows other packing subregions to form random microstructures. That is why packings are considered to be in a coexistence region for densities above φ_C.[11,43]

Finally, the pore-size entropy in Fig. 3 starts decreasing again at higher packing densities (beyond $\varphi \approx 0.68$). It corresponds to the exhaustion of available packing configurations, which were released after the onset of the crystallization process. Indeed, if a particle resides in a dilute crystalline packing, it can be shifted slightly, thus exploring the phase space. After packing contraction the given particle can be shifted only by a smaller distance, which indicates a lower number of available states.

B Comparison with other measures

For a better interpretation of the results in Fig. 3, we present in Fig. 4 several other well-known measures that were computed for the same packings. First, we construct Voronoi volumes around particle centers and record their standard deviation (Fig. 4a).[8,69] The structural transition is determined by the local minimum of the density–measure plot. Second, the entropy is

computed over the given Voronoi volumes according to the hard spheres' statistical mechanics formalism[1,6,17] (Fig. 4b). Similarly, the local minimum of the function exposes the structural transition. Third, we analyze a local bond-orientational order measure Q_6^{local} (Fig. 4c),[70] used in several papers.[11,46,63,71] A steep increase of order indicates the structural transition. Finally, we utilize the geometrical coordination number metric z (Fig. 4d),[11] also employed and investigated in several publications.[54,56,72] To estimate the number of geometrical contacts in a packing we contract the packing uniformly with a linear strain rate equal to 10^{-3} and count particle intersections introduced during contraction. For the coordination numbers the structural transition should be tracked from the start of the plateau, when z approaches 6 (the coordination number for isostatic packings of frictionless particles), which indicates the frictionless jamming transition.

All of the complementary measures (Fig. 4) demonstrate good coincidence with the results from the original papers and also expose the structural transition at critical packing densities of $\varphi_C = 0.647$–0.651, with the exact value depending on the actual measure, the packing type, and some uncertainty resulting from noise.

We point out a very similar behavior of all the entropy-like measures: of pore-size entropy in Fig. 3, of the Voronoi volumes standard deviation in Fig. 4a, and of the Voronoi volumes entropy in Fig. 4b. The measures decrease as φ is increased up to φ_C, increase in the coexistence region, and thereafter start decreasing again. The reasons for this behavior were analyzed above for the pore-size entropy. The similarity between pore-size entropy and the Voronoi volumes entropy may explain the interdependence between the Voronoi volumes' distribution shape parameter "k" and the pore-size distribution's standard deviation.[25]

The different packing types we used (LS, JT, and force-biased algorithms) demonstrate significantly different values for most of the measures below φ_C (Fig. 3 and 4). All entropy-like measures and the local bond-orientational order measure show that LS packings are the most disordered ones among the studied packing types (*i.e.*, the entropies and Voronoi volumes standard deviations are the highest; local bond-orientational order is the lowest); JT packings are the least disordered packings, and FBA packings have intermediate disorder. It means that the different packing generation protocols result in different microstructures. This is very important, because the packing microstructure affects flow and mass transport in the packings, as visualized in the effective diffusivity (or diffusive tortuosity) and hydrodynamic dispersion, as well as the elastic (and other bulk) properties of the packings.[25,26,69,73–78] Moreover, the differences in the pore-size entropy values for monodisperse packings at identical packing densities demonstrate that the pore-size distribution depends on the packing microstructure (thus, on the packing generation protocol) and cannot be approximated with a function that depends only on the packing density, *e.g.*, using Carnahan–Starling or Percus–Yevick equations of state.[20–22]

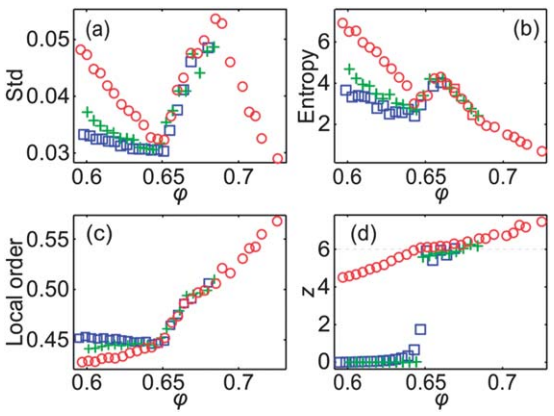

Fig. 4 Complementary packing measures *vs.* packing density φ applied to the same monodisperse sphere packings as in Fig. 3 generated with the Lubachevsky–Stillinger algorithm (○), a force-biased algorithm (+), and the Jodrey–Tory algorithm (□). (a) Standard deviation of Voronoi volumes; (b) entropy of Voronoi volumes; (c) local bond-orientational order; and (d) geometrical coordination number.

Another remarkable feature of these sphere packings, which were generated with different packing protocols, is the similarity of measure values at densities above φ_C (Fig. 3 and 4). This supports the idea that the behavior of the packing properties becomes indistinguishable at this critical density and beyond.[50] Unsurprisingly, the origin of a packing regarding its generation protocol ultimately disappears.

The differences in pore-size entropy observed for the different packing types at identical packing densities below φ_C in Fig. 3 can be explained in terms of the geometrical coordination number. The slope of the density–entropy plot indicates the depletion rate at increasing packing density of the phase space volume available for the packings. The more near-neighbors the particles have in a packing, the more restrictions are imposed on the particle movement, and the less possibilities exist for contracting the packing of a given density to reach a slightly higher density, *i.e.*, the less phase space paths emanate from the current packing hyperstate in the phase space. Thus, packings with higher geometrical coordination number should exhibit a more negative slope in their density–entropy plot. As far as the pore-size entropy plots converge to the same value at φ_C for all packing types in Fig. 3, we conclude that packings with higher geometrical coordination number should have higher entropy values (and any other disorder measures) for densities below φ_C. This behavior is indeed reported for the cases in Fig. 3 and 4.

An important consequence of the applicability of the pore-size entropy is the justification of the slicing assumption explained in Section III. As long as the pore-size distribution approach reproduces the expected entropy behavior, we may conclude that each packing of N particles represents a slice in the phase space of the $N + 1$ particles, and the density of available states of this slice is equal to that of the available states of the whole packing phase space (eqn (3)).

Of course, sphere packings in the entire range of density can also be constructed from a perfectly crystalline configuration just by an appropriate decrease of the particle diameter. In this case, pore-size entropy will be monotonically decreasing. The observed non-monotonic behavior in Fig. 3 is explained in the

following way: up to φ_C the phase space is dominated by the basins of attraction of random configurations and any algorithm, starting its operation from a random particle distribution, will hardly encounter an ordered packing. Above φ_C, the coexistence region starts and the basins of attraction of crystalline configurations occupy a significant amount of the phase space (compared to the random configurations). As a consequence, sufficiently large packings will be composed of both ordered and disordered subregions, representing the coexistence phenomenon. The calculated total entropy value will be comprised of entropies from ordered and disordered regions weighted by their relative volumes.[79]

One can consider an entire packing as a large number of smaller sub-packings, each of them probing a phase space with lower dimensionality. We can roughly estimate the number of independent smaller packings in a large one by employing a pair-correlation function.[11,43,80] If we assume that the correlations disappear at a distance of three particle diameters, the volume of an independent sub-packing is $4/3 \times \pi(6r_0)^3$. The total volume of a packing of 10 000 particles with $\varphi = 0.64$ is $10\,000 \times 4/3 \times \pi r_0^3/0.64$. Therefore, the number of independent sub-packings is 72, which provides sufficient statistics for probing both crystalline and random phase space regions.

C Random-close packing limit

It is tempting to attribute the critical density $\varphi_C = 0.647$–0.651 to the RCP limit, as the pore-size entropy has a profound minimum in this interval, indicating a minimal amount of available states (Fig. 3). Yet, these densities differ somewhat from the generally accepted RCP limit $\varphi_{RCP} \approx 0.64$ obtained in experiments and by direct generation of jammed configurations,[8,11,37–42] but they are close to the claimed RCP limit $\varphi = 0.646$–0.65 detected by structural changes in packings (*e.g.*, as analyzed from the local entropy minimum or onset of crystallization),[1–6] which is also supported theoretically.[81] The density for mechanically stable packings of almost frictionless particles, reported by Briscoe *et al.*[12] (*cf.* Fig. 2 in that paper), is also larger than $\varphi_{RCP} \approx 0.64$ and actually equal to 0.645. However, it may happen that a structural transition in a packing, *e.g.*, as indicated by the local entropy minimum in Fig. 3, reflects a phenomenon that is unrelated to the RCP limit and occurs at a density slightly above φ_{RCP}.[3]

In pursuit of a better understanding of these observations we examine the LS packings under fast compressions. It is argued that monosized packings in the course of fast compressions (or fast quenching in energy minimization protocols) should avoid crystallization and jam at φ_{RCP}.[40] Still, LS packings seem to jam in a wide range of density even for fast compressions.[62] Another problem with jamming of LS packings is that these packings at low densities have coordination numbers as low as 4, meaning that they are not yet jammed (*cf.* Fig. 4d), though Salsburg and Wood[61] showed analytically that isostaticity of a subset of particles in a packing (excluding rattler particles) is a necessary condition for infinite pressure. To address these points we follow the idea of Skoge *et al.*[62] and additionally densify packings obtained with the LS protocol in the density range of $\varphi_{initial} = 0.635$–$0.65$ (compression rates span from 1.2×10^{-2} to 2.5×10^{-4}, respectively). The densification is accomplished by applying the LS protocol to these packings again, but now with a low compression rate (10^{-5}), which would lead to crystalline configurations if used from the very beginning of the packing generation. The dependence of the final packing densities on the initial ones is shown in Fig. 5a (different symbols represent different regimes discussed below). It demonstrates that packings with $\varphi_{initial} < 0.64$ (below the usually accepted RCP limit) can be compressed further to reach densities in the interval $\varphi_{final} = 0.641$–0.644, which is indeed very close to φ_{RCP}.

To understand the densification process better, we plot the reduced pressure in several packings in the course of slow compression in Fig. 5b. All the lines should be tracked from left to right, and the leftmost point of each line represents the initial density and pressure. We notice that the pressure rapidly drops in all cases, then recovers and finally reaches the termination value (10^{12}) again. The pressure drop happens due to the packing equilibration during slow compression, meaning that

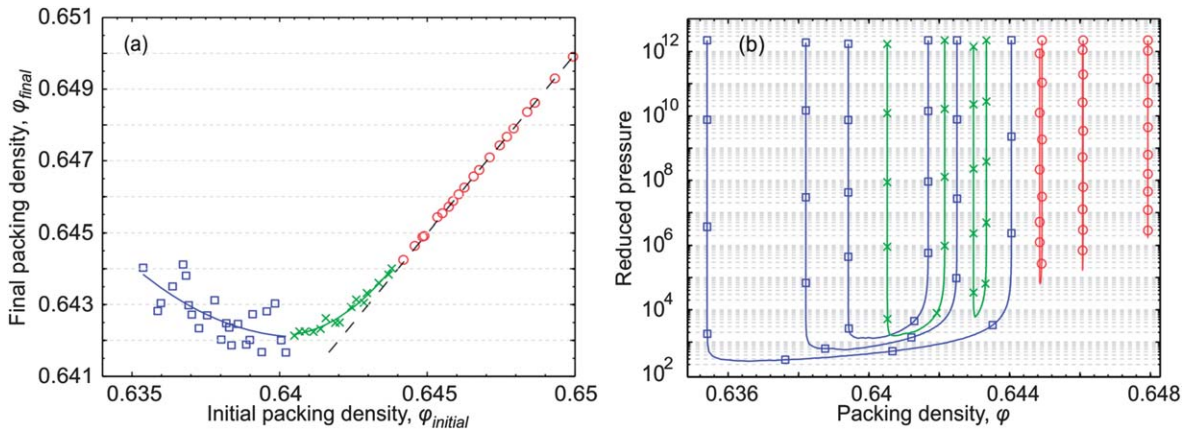

Fig. 5 The Lubachevsky–Stillinger algorithm applied with slow compression to packings initially generated with the same algorithm, but under faster compressions. (a) Final *vs.* initial packing densities: unjammed packings below the RCP limit (blue squares), jammed packings above the RCP limit (red circles), and intermediate regime (green crosses); $\varphi_{final} = \varphi_{initial}$ reference line (dashed black line). Solid lines are least-squares quadratic fits for data of the corresponding color. (b) Pressure *vs.* packing density for selected packings in the course of slow compression with the Lubachevsky–Stillinger algorithm. Colors and symbols correspond to panel (a).

packing structures after fast compressions are out of equilibrium. During equilibration particles collide and fill the packing space more evenly to increase the average cage size per particle and reduce the number of collisions per unit time. The slower is the compression during the generation of the initial LS packings (and the higher φ_{initial}), the smaller is the pressure drop, because slower compressions produce better equilibrated packings.

The presented picture resolves an apparent controversy with the LS algorithm: a necessary and sufficient condition for infinite pressure in hard-sphere packings is isostaticity,[61] though for low densities the LS packings expose coordination numbers as low as 4 and still possess very high pressure at the algorithm termination (Fig. 4d). We have shown in Fig. 5b that this pressure represents non-equilibrium and should not be used either for the tracking of jamming or for the estimation of jamming densities, as done in several papers.[13,62,82] Instead, the packings should be preliminarily equilibrated at zero (or a very low) compression rate. We also verified that the average number of contacts per sphere computed at a strain rate of 10^{-4} is $5.9 < z < 6$ for all the densified packings, if rattler particles with less than four contacts were recursively removed. The pressure drop also explains the ability to further compress packings with $\varphi_{\text{initial}} < 0.64$, which initially seemed to be jammed and kinetically arrested.

We notice that the lower the φ_{initial} (if it is below 0.6405), the higher the φ_{final}, *i.e.*, the blue-square data in Fig. 5a have a negative slope (the least-squares quadratic fit is shown as a solid blue line). The blue-colored pressure plots shown in Fig. 5b also demonstrate this tendency. It can easily be explained assuming that trapping of a packing in the least dense glassy states (φ_{d} in the review by Parisi and Zamponi,[43] Fig. 4) happens at a density of $\varphi \approx 0.64$. Packings that start the slow compression at lower densities have more time for structural rearrangement (before they reach φ_{d}) and can longer avoid trapping in the glassy states above φ_{d}.

Data in Fig. 5a for $\varphi_{\text{initial}} \geq 0.644$ (red circles) almost coincide with the $\varphi_{\text{final}} = \varphi_{\text{initial}}$ reference (dashed black line). It means that packings are already kinetically arrested in glassy states, though pressure drops still take place due to the non-equilibrium structure of the packings (red lines in Fig. 5b). We also verified that the lowest pressure value for quasistatic compressions of all packings in Fig. 5 is equal to the stationary reduced pressure. To determine the latter, we equilibrated packings by performing sets of 2×10^4 collisions with zero compression rate in a loop until the relative difference of reduced pressures in the last two sets is less than 10^{-4}. Therefore, packings with $\varphi_{\text{initial}} \geq 0.644$ are nearly jammed also by pressure criteria (as we mentioned, according to Salsburg and Wood[61] packings close to jamming should exhibit very high stationary reduced pressure; the lowest pressure for $\varphi_{\text{initial}} \geq 0.644$ in Fig. 5 is larger than 10^4, which we consider as sufficiently high). The proximity to jamming can be verified by the equation of state for hard spheres of Salsburg and Wood,[61] $p = d/(1 - \varphi/\varphi_{\text{J}})$, where p is the stationary reduced pressure, φ is the current packing density, φ_{J} is the closest jamming density achievable from the given packing configuration (which we would like to estimate), and d is the dimensionality of the system. We obtain $\varphi_{\text{J}} = \varphi/(1 - d/p) \approx \varphi(1 + d/p)$. φ_{J} for $\varphi_{\text{initial}} = 0.644$ is ~0.6442. We note that the method for testing mechanical stability by pressure is equivalent to the dynamical matrix test[41] or linear programming methods[49] due to the results of Salsburg and Wood.[61] The benefit of the pressure test lies in our ability to explicitly estimate the quality of the threshold by assessing the difference between expected jamming densities and actual densities of the packings we consider as jammed (through the equation of state by a given threshold, as just done for $\varphi = 0.644$).

The remaining part of the plot in Fig. 5a (green crosses) lies in the density range [0.6405, 0.644). This plot does not coincide with the $\varphi_{\text{final}} = \varphi_{\text{initial}}$ line (packings are not yet kinetically arrested), but has a positive slope smaller than unity (the least-squares quadratic fit is depicted by a solid green line). The lower the φ_{initial}, the larger the difference between φ_{final} and φ_{initial} (see also the green lines in Fig. 5b). At least one of the following two scenarios is possible, or both are taking place: (i) the packings are initially trapped in glassy states and slightly rearrange due to equilibration to fill the space more evenly, which provides opportunities for further densification and kinetic arrest; and (ii) packings do not initially reside in glassy states and become trapped in the course of densification. Packings with higher φ_{initial} are trapped earlier, which may happen because the higher is the density, the closer is the packing structure to glassy states, and the density of glassy states in the phase space increases with the packing density. To determine the actual scenario it is necessary to compare the packing structures before and after densification by, *e.g.*, Delaunay network graph isomorphism[12] or the distance between packing configurations in the phase space (normalized to a single density). However, this is beyond the scope of the present paper.

Our analysis suggests that φ_{d} as well as φ_{RCP} (infinite-pressure limit of φ_{d}) are close to 0.64. The problem with the traditional LS algorithm is that fast compressions terminate too early due to the non-equilibrium pressure excess and slow compressions are able to reach densities above the RCP limit due to crystallization. To improve our φ_{RCP} estimate, we modified the LS generation procedure and after every 2×10^4 collisions with compression we completely equilibrate the packings. The equilibration is done by performing sets of 2×10^4 collisions with zero compression rate in a loop until the relative difference of reduced pressures in the last two sets is less than 1%, so the pressure is stationary. When a packing is equilibrated we perform collisions with compression again. We terminate the generation process when the stationary reduced pressure is high enough (10^{12}).

Two sets of data were generated with this modification: six packings with a compression rate of 0.04 and six packings with a compression rate of 0.1; previously generated LS packings in the density range $\varphi = 0.62$–0.623 were used as starting configurations. All of the packings jam in the density range $\varphi = 0.639$–0.641 and are indeed nearly isostatic (*i.e.*, the average number of contacts per sphere computed at a strain rate of 10^{-4} is $5.98 < z < 6$, if rattler particles with less than four contacts are recursively removed). This clearly corresponds to the usually accepted

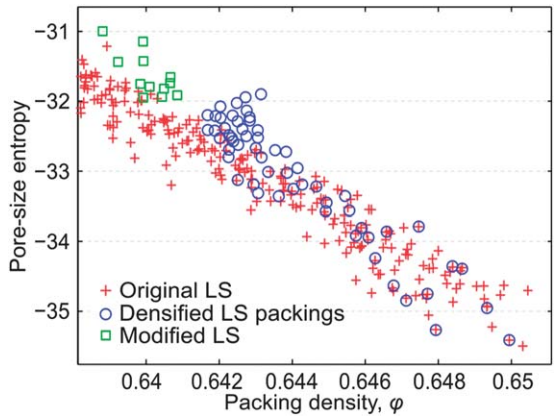

Fig. 6 Pore-size entropy *vs.* packing density for three types of Lubachevsky–Stillinger (LS) packings: original data from Fig. 3 (+); packings densified with slow compression (○); and packings used to estimate the RCP limit with the modified LS algorithm (□).

estimate of the RCP limit and is also consistent with our previous discussion. The RCP limit estimates for the two datasets with 5% confidence intervals are respectively $\varphi_{RCP} = 0.6401 \pm 0.0008$ and $\varphi_{RCP} = 0.64 \pm 0.0005$. Both datasets are found to belong to the same distribution and we estimate the RCP limit from the combined data to be $\varphi_{RCP} = 0.6401 \pm 0.0004$. We are not aware of such a precise RCP limit estimation for the LS protocol. Our approach also benefits greatly from the ability to recover both characteristic densities (~0.64 and ~0.65) for the same protocol (Lubachevsky-Stillinger algorithm), which has not yet been done, to our knowledge. We conjecture that in the thermodynamic limit any single packing generation with the modified LS algorithm will terminate at φ_{RCP}.[40] We have also already shown an explicit way to produce jammed packings above φ_{RCP} (though the LS algorithm by itself produces jammed packings only for $\varphi \geq 0.644$): one needs to further densify packings of lower densities by slow compression (as in Fig. 5).

To complete the discussion on these additionally generated packings, we plot pore-size entropy *vs.* packing density in Fig. 6 for LS packings densified with the slow compression ("Densified LS packings", see also Fig. 5), as well as for the packings used to estimate the RCP limit by employing the modified LS algorithm ("Modified LS"). We also depict entropies for the packings from the original LS algorithm (see Fig. 3) for a better interpretation. Unsurprisingly, densified packings for $\varphi \geq 0.644$ (*cf.* red circles in Fig. 5) have their entropy unchanged in comparison to the original LS packings, as their density and structure are retained. Densified packings with a final density below 0.644 (blue squares and green crosses in Fig. 5) and packings from the modified algorithm have entropies slightly above those for the original LS packings (Fig. 6). This agrees with our prediction from Section IV, part B, where it was stated that "packings with higher geometrical coordination number should have higher entropy values for densities below φ_C". Indeed, the densified LS packings and modified LS packings are truly isostatic, whereas the original LS packings with $\varphi < 0.644$ are not isostatic.

The results in Fig. 6 also show that the RCP limit conforms to the "maximally random jammed state" definition.[47] Indeed, random packings (*i.e.*, without crystalline regions) have densities below $\varphi_C \approx 0.65$, and random jammed packings occupy the density range from φ_{RCP} to φ_C. The maximally random state of these random jammed states has a density $\varphi_{RCP} \approx 0.64$, because entropy decreases in this density range, as depicted in Fig. 6. Therefore, the definition of the RCP limit we use in this paper is equivalent to the maximally random jammed state definition.

D Structural transition

We conclude that the critical density of the structural transition $\varphi_C = 0.647$–0.651, as determined by the pore-size entropy (Fig. 3) and the complementary measures (Fig. 4), does not represent the density of the RCP limit defined *via* the infinite-pressure limit of the least dense glassy states.[43]

We conjecture that $\varphi_C = 0.647$–0.651 represents φ_{GCP},[43] the infinite-pressure limit of the densest glassy state (the ideal glass state). This last glassy state itself is encountered at finite pressure at the Kauzmann density φ_K, which is lower than φ_{GCP}.

On the other hand, it is believed that the configurational entropy for jammed packings becomes zero at φ_{GCP}, whereas the pore-size entropy should tend to minus infinity (when p_{avail} in eqn (2) tends to zero). For LS packings (as the most jammed of all the studied packing types, Fig. 4d) the pore-size entropy plot in Fig. 3 and the Voronoi volumes entropy plot in Fig. 4b can be extrapolated at φ_C (toward higher density) to minus-infinity and zero, respectively, which leads to $\varphi_{GCP} \approx 0.66$ (it is also called Kauzmann density in the original paper for the Voronoi volumes entropy[1]).

Therefore, the above conjecture $\varphi_C = \varphi_{GCP}$ has the following inconsistencies: (i) both entropies (pore-size entropy and Voronoi volumes entropy) do not reach the expected minimum values at φ_C, they can only be inferred by extrapolation; (ii) replica theory estimates φ_K to be 0.62 and φ_{GCP} to be 0.68.[43] Still, replica theory may be imprecise and there is an analytical theory which predicts the configurational entropy to disappear at $\varphi = 0.65$ (*cf.* Fig. 2 in the study of Aste and Coniglio[81]). Furthermore, finite-size effects are believed to shift φ_K and φ_{GCP} to lower values. Finally, too high entropy values at $\varphi_C = \varphi_{GCP}$ in Fig. 3 and 4b can be justified with the following arguments: (i) the entropies also account for unjammed packings with the same density; (ii) rattler particles and their flexibility in position also contribute to the entropies; and (iii) both entropies involve some approximations, which may lead to overestimated entropy values.

Another possibility is that the density φ_C simply represents the last achievable jammed state, after which crystalline regions are unavoidable, but φ_{GCP} is still not reached. The location of φ_K is also arguable; it may be at $\varphi = 0.66$ as well. We reject this conjecture ($\varphi_C < \varphi_{GCP}$) by the following arguments: (i) we once again refer to the analytical prediction for the configurational entropy to vanish at $\varphi = 0.65$;[81] (ii) the density $\varphi_C \approx 0.65$, which we obtained by different measures for different packing protocols (Fig. 3 and 4), has a universal character; and (iii) $\varphi_C \approx 0.65$ fits very well into the plot for maximal packing densities of polydisperse particles reported by Hermes and Dijkstra[82] (their

Fig. 4b, compression rate 10^{-5}). It means that crystalline configurations are not only more probable for $\varphi > 0.65$, but that amorphous jammed states cannot be reached for higher φ (even if we could suppress crystallization). Therefore, we conjecture that $\varphi_C = 0.647$–0.651 represents φ_{GCP}, the infinite-pressure limit of the densest glassy state (the ideal glass state).

V Summary and conclusions

We have introduced and analyzed a pore-size entropy measure for random packings of hard spheres. It reproduces the structural transition of monodisperse sphere packings, has a clear physical background, is numerically efficient, does not require *a priori* parameters, *e.g.*, a characteristic length, and can easily be applied also to polydisperse sphere packings. In addition, this measure provides important insight into the pore-size distribution of the packings; specifically, the logarithm of its tail area is equal to the packing entropy.

The applied pore-size entropy measure indicates a structural transition of monodisperse packings of frictionless spheres at a critical density of $\varphi_C \approx 0.65$, corresponding to a minimal number of available packing states, *i.e.*, to the local entropy minimum. This minimum is followed by an entropy increase in the coexistence region up to $\varphi \approx 0.68$; above this packing density the entropy starts decreasing again.

We amended the Lubachevsky–Stillinger packing generation protocol to systematically reproduce the RCP limit at $\varphi_{RCP} \approx 0.64$ for fast compressions. We are not aware of reports that recover both characteristic densities ($\sim$0.64 and $\sim$0.65) by using the same protocol. This result suggests that the structural transition at $\varphi_C \approx 0.65$ and the RCP limit at $\varphi_{RCP} \approx 0.64$ are unrelated phenomena and cannot be justified by a difference in preparation protocols. We explain this observation on the basis of a picture proposed in a review by Parisi and Zamponi.[43] While $\varphi_{RCP} \approx 0.64$ corresponds to the jammed configurations of the least dense glassy states (φ_{th} in this review), $\varphi_C \approx 0.65$ corresponds to the jammed configuration of the densest glassy state (φ_{GCP} in this review).

The significantly different pore-size entropy plots at packing densities below the structural transition density observed for the different protocols (Lubachevsky–Stillinger, Jodrey–Tory, force-biased algorithms) prove that the packing microstructure and pore-size distribution at a given φ depend intrinsically on the packing generation protocol. The pore-size entropy is a powerful measure to detect and quantify protocol-specific packing disorder, which is known to impact upon key bulk and transport properties of random sphere packings encountered in materials science and industrial engineering, *e.g.*, in the processing of ceramics or the operation of fixed-bed chemical reactors and chromatographic columns. In the future we will apply the presented approach to particle size distributions (and polydisperse packings) relevant to these applications.

Acknowledgements

This work was supported by the Deutsche Forschungsgemeinschaft DFG (Bonn, Germany) under grant TA 268/5-1. We are grateful to the John von Neumann Institute for Computing (NIC) and the Jülich Supercomputing Center (JSC) for the allocation of special CPU-time grants (NIC project numbers: 4717 and 5658, JSC project ID: HMR10). We also thank the reviewers for their extremely helpful and stimulating comments.

References

1 A. V. Anikeenko, N. N. Medvedev and T. Aste, *Phys. Rev. E: Stat., Nonlinear, Soft Matter Phys.*, 2008, **77**, 031101.
2 A. V. Anikeenko and N. N. Medvedev, *Phys. Rev. Lett.*, 2007, **98**, 235504.
3 S. C. Kapfer, W. Mickel, K. Mecke and G. E. Schröder-Turk, *Phys. Rev. E: Stat., Nonlinear, Soft Matter Phys.*, 2012, **85**, 030301.
4 B. A. Klumov, S. A. Khrapak and G. E. Morfill, *Phys. Rev. B: Condens. Matter Mater. Phys.*, 2011, **83**, 184105.
5 M. Bargieł and E. M. Tory, *Adv. Powder Technol.*, 2001, **12**, 533–557.
6 T. Aste and T. Di Matteo, *Eur. Phys. J. B*, 2008, **64**, 511–517.
7 S. F. Edwards and R. B. S. Oakeshott, *Phys. A*, 1989, **157**, 1080–1090.
8 C. Song, P. Wang and H. A. Makse, *Nature*, 2008, **453**, 629–632.
9 C. Briscoe, C. Song, P. Wang and H. A. Makse, *Phys. Rev. Lett.*, 2008, **101**, 188001.
10 P. Wang, C. Song, Y. Jin and H. A. Makse, *Phys. A*, 2011, **390**, 427–455.
11 Y. Jin and H. A. Makse, *Phys. A*, 2010, **389**, 5362–5379.
12 C. Briscoe, C. Song, P. Wang and H. A. Makse, *Phys. A*, 2010, **389**, 3978–3999.
13 A. Donev, F. H. Stillinger and S. Torquato, *J. Chem. Phys.*, 2007, **127**, 124509.
14 V. S. Kumar and V. Kumaran, *J. Chem. Phys.*, 2005, **123**, 114501.
15 R. Blumenfeld and S. F. Edwards, *Phys. Rev. Lett.*, 2003, **90**, 114303.
16 S. Henkes, C. S. O'Hern and B. Chakraborty, *Phys. Rev. Lett.*, 2007, **99**, 038002.
17 T. Aste and T. Di Matteo, *Phys. Rev. E: Stat., Nonlinear, Soft Matter Phys.*, 2008, **77**, 021309.
18 S. S. Ashwin and R. K. Bowles, *Phys. Rev. Lett.*, 2009, **102**, 235701.
19 P. V. Giaquinta and G. Giunta, *Phys. A*, 1992, **187**, 145–158.
20 S. Torquato, B. Lu and J. Rubinstein, *Phys. Rev. A: At., Mol., Opt. Phys.*, 1990, **41**, 2059–2075.
21 B. Lu and S. Torquato, *Phys. Rev. A: At., Mol., Opt. Phys.*, 1992, **45**, 5530–5544.
22 S. Torquato, *Phys. Rev. E: Stat. Phys., Plasmas, Fluids, Relat. Interdiscip. Top.*, 1995, **51**, 3170–3182.
23 M. Alonso, E. Sainz, F. A. Lopez and K. Shinohara, *Chem. Eng. Sci.*, 1995, **50**, 1983–1988.
24 M. Alonso, M. Satoh and K. Miyanami, *Can. J. Chem. Eng.*, 1992, **70**, 28–32.
25 I. Schenker, F. T. Filser, L. J. Gauckler, T. Aste and H. J. Herrmann, *Phys. Rev. E: Stat., Nonlinear, Soft Matter Phys.*, 2009, **80**, 021302.

26 I. Schenker, F. Filser, M. Hütter and L. Gauckler, *Granular Matter*, 2012, **14**, 333–340.
27 S. Torquato, *Annu. Rev. Mater. Res.*, 2002, **32**, 77–111.
28 D. Stoyan, A. Wagner, H. Hermann and A. Elsner, *J. Non-Cryst. Solids*, 2011, **357**, 1508–1515.
29 A. Donev, S. Torquato and F. H. Stillinger, *J. Comput. Phys.*, 2005, **202**, 765–793.
30 A. V. Kyrylyuk, M. A. van de Haar, L. Rossi, A. Wouterse and A. P. Philipse, *Soft Matter*, 2011, **7**, 1671–1674.
31 K. Wang, C. Song, P. Wang and H. A. Makse, *Phys. Rev. E: Stat., Nonlinear, Soft Matter Phys.*, 2012, **86**, 011305.
32 B. D. Lubachevsky and F. H. Stillinger, *J. Stat. Phys.*, 1990, **60**, 561–583.
33 W. S. Jodrey and E. M. Tory, *Phys. Rev. A: At., Mol., Opt. Phys.*, 1985, **32**, 2347–2351.
34 M. Bargieł and J. Mościński, *Comput. Phys. Commun.*, 1991, **64**, 183–192.
35 J. Mościński, M. Bargieł, Z. A. Rycerz and P. W. M. Jacobs, *Mol. Simul.*, 1989, **3**, 201–212.
36 A. Bezrukov, M. Bargieł and D. Stoyan, *Part. Part. Syst. Charact.*, 2002, **19**, 111–118.
37 J. D. Bernal, *Nature*, 1960, **185**, 68–70.
38 J. D. Bernal and J. Mason, *Nature*, 1960, **188**, 910–911.
39 C. S. O'Hern, S. A. Langer, A. J. Liu and S. R. Nagel, *Phys. Rev. Lett.*, 2002, **88**, 075507.
40 C. S. O'Hern, L. E. Silbert, A. J. Liu and S. R. Nagel, *Phys. Rev. E: Stat., Nonlinear, Soft Matter Phys.*, 2003, **68**, 011306.
41 N. Xu, J. Blawzdziewicz and C. S. O'Hern, *Phys. Rev. E: Stat., Nonlinear, Soft Matter Phys.*, 2005, **71**, 061306.
42 G. D. Scott and D. M. Kilgour, *J. Phys. D: Appl. Phys.*, 1969, **2**, 863.
43 G. Parisi and F. Zamponi, *Rev. Mod. Phys.*, 2010, **82**, 789–845.
44 G.-J. Gao, J. Bławzdziewicz and C. S. O'Hern, *Phys. Rev. E: Stat., Nonlinear, Soft Matter Phys.*, 2006, **74**, 061304.
45 C. F. Schreck, C. S. O'Hern and L. E. Silbert, *Phys. Rev. E: Stat., Nonlinear, Soft Matter Phys.*, 2011, **84**, 011305.
46 S. Torquato and F. H. Stillinger, *Rev. Mod. Phys.*, 2010, **82**, 2633–2672.
47 S. Torquato, T. M. Truskett and P. G. Debenedetti, *Phys. Rev. Lett.*, 2000, **84**, 2064.
48 A. Donev, *J. Appl. Phys.*, 2004, **95**, 989–999.
49 A. Donev, S. Torquato, F. H. Stillinger and R. Connelly, *J. Comput. Phys.*, 2004, **197**, 139–166.
50 P. Chaudhuri, L. Berthier and S. Sastry, *Phys. Rev. Lett.*, 2010, **104**, 165701.
51 S. Alexander, *Phys. Rep.*, 1998, **296**, 65–236.
52 N. Xu and E. S. C. Ching, *Soft Matter*, 2010, **6**, 2944–2948.
53 H. A. Makse, D. L. Johnson and L. M. Schwartz, *Phys. Rev. Lett.*, 2000, **84**, 4160–4163.
54 P. Wang, C. Song, Y. Jin, K. Wang and H. A. Makse, *J. Stat. Mech.: Theory Exp.*, 2010, P12005.
55 C. F. Moukarzel, *Phys. Rev. Lett.*, 1998, **81**, 1634–1637.
56 A. Donev, S. Torquato and F. H. Stillinger, *Phys. Rev. E: Stat., Nonlinear, Soft Matter Phys.*, 2005, **71**, 011105.
57 L. E. Silbert, *Soft Matter*, 2010, **6**, 2918–2924.
58 A. Mehta, *Soft Matter*, 2010, **6**, 2875–2883.
59 C. B. O'Donovan and M. E. Möbius, *Phys. Rev. E: Stat., Nonlinear, Soft Matter Phys.*, 2011, **84**, 020302.
60 I. Biazzo, F. Caltagirone, G. Parisi and F. Zamponi, *Phys. Rev. Lett.*, 2009, **102**, 195701.
61 Z. W. Salsburg and W. W. Wood, *J. Chem. Phys.*, 1962, **37**, 798–804.
62 M. Skoge, A. Donev, F. H. Stillinger and S. Torquato, *Phys. Rev. E: Stat., Nonlinear, Soft Matter Phys.*, 2006, **74**, 041127.
63 K. Lochmann, A. Anikeenko, A. Elsner, N. Medvedev and D. Stoyan, *Eur. Phys. J. B*, 2006, **53**, 67–76.
64 N. Xu, D. Frenkel and A. J. Liu, *Phys. Rev. Lett.*, 2011, **106**, 245502.
65 S. S. Ashwin, J. Blawzdziewicz, C. S. O'Hern and M. D. Shattuck, *Phys. Rev. E: Stat., Nonlinear, Soft Matter Phys.*, 2012, **85**, 061307.
66 A. C. Cohen, *Ann. Math. Stat.*, 1950, **21**, 557–569.
67 M. Abramowitz and I. A. Stegun, *Handbook of Mathematical Functions: With Formulas, Graphs, and Mathematical Tables*, Dover Publications, New York, 1965.
68 G.-J. Gao, J. Blawzdziewicz, C. S. O'Hern and M. D. Shattuck, *Phys. Rev. E: Stat., Nonlinear, Soft Matter Phys.*, 2009, **80**, 061304.
69 S. Khirevich, A. Daneyko, A. Höltzel, A. Seidel-Morgenstern and U. Tallarek, *J. Chromatogr., A*, 2010, **1217**, 4713–4722.
70 P. J. Steinhardt, D. R. Nelson and M. Ronchetti, *Phys. Rev. B*, 1983, **28**, 784–805.
71 K. Lochmann, L. Oger and D. Stoyan, *Solid State Sci.*, 2006, **8**, 1397–1413.
72 G. W. Delaney, T. D. Matteo and T. Aste, *Soft Matter*, 2010, **6**, 2992–3006.
73 S. Khirevich, A. Höltzel, A. Daneyko, A. Seidel-Morgenstern and U. Tallarek, *J. Chromatogr., A*, 2011, **1218**, 6489–6497.
74 D. Hlushkou, S. Khirevich, V. Apanasovich, A. Seidel-Morgenstern and U. Tallarek, *Anal. Chem.*, 2007, **79**, 113–121.
75 A. Daneyko, S. Khirevich, A. Höltzel, A. Seidel-Morgenstern and U. Tallarek, *J. Chromatogr., A*, 2011, **1218**, 8231–8248.
76 V. A. Buryachenko, N. J. Pagano, R. Y. Kim and J. E. Spowart, *Int. J. Solids Struct.*, 2003, **40**, 47–72.
77 S. Khirevich, A. Höltzel, A. Seidel-Morgenstern and U. Tallarek, *J. Chromatogr., A*, 2012, **1262**, 77–91.
78 S. Khirevich, A. Höltzel and U. Tallarek, *Commun. Comput. Phys.*, 2013, **13**, 801–822.
79 C. Radin, *J. Stat. Phys.*, 2008, **131**, 567–573.
80 T. Aste, M. Saadatfar and T. J. Senden, *Phys. Rev. E: Stat., Nonlinear, Soft Matter Phys.*, 2005, **71**, 061302.
81 T. Aste and A. Coniglio, *Europhys. Lett.*, 2004, **67**, 165–171.
82 M. Hermes and M. Dijkstra, *Europhys. Lett.*, 2010, **89**, 38005.

